Available online at www.sciencedirect.com
SCIENCE DIRECT
Icarus 181 (2006) 223–234
ICARUS
www.elsevier.com/locate/icarus

Cassini ISS astrometric observations of the inner jovian satellites, Amalthea and Thebe

N.J. Cooper [a,*], C.D. Murray [a], C.C. Porco [b], J.N. Spitale [b]

[a] *Astronomy Unit, School of Mathematical Sciences, Queen Mary, University of London, Mile End Road, London, E1 4NS, UK*
[b] *Cassini Imaging Central Laboratory for Operations, Space Science Institute, 4750 Walnut Street, Suite 205, Boulder, CO 80301, USA*

Received 27 June 2005; revised 28 October 2005

Available online 15 December 2005

Abstract

We present a total of 289 new astrometric observations of the inner jovian satellites, Amalthea and Thebe, obtained using the Cassini ISS narrow angle camera. Observations were made using image sequences from 2000 December 11–12 (inbound) and 2001 January 15–16 (outbound), at phase angles of approximately 2° and 122°, respectively. Target distances were of order 284 R_J, giving a maximum resolution of approximately 100 km/pixel. Centroided line and sample values for 239 observations of Amalthea and 50 of Thebe are provided, together with estimated camera pointing information for each image. Orbit fitting using a uniformly precessing Keplerian ellipse model, taking into account the oblateness of Jupiter up to terms in J_6, gave RMS fit residuals of 0.364 and 0.443 pixel for Amalthea and Thebe, respectively (equivalent to 0.450 and 0.547 arcsec). RMS residuals relative to the JPL JUP230 ephemeris were 0.306 and 0.604 pixel (equivalent to 0.378 and 0.746 arcsec), for Amalthea and Thebe. The fitted orbital parameters confirm the relatively high inclinations of these satellites (0.374° ± 0.002° and 1.076° ± 0.003°, respectively), equivalent to maximum vertical displacements above Jupiter's equatorial plane of 1188 ± 6 and 4240 ± 12 km, respectively, consistent with current estimates of the half-thicknesses of the Amalthea and Thebe gossamer rings [Ockert-Bell, M.E., Burns, J.A., Dauber, I.J., Thomas, P.C., Veverka, J., Belton, M.J.S., Klaasen, K.P., 1999. Icarus 138, 188–213].

Keywords: Satellites, general; Satellites of Jupiter; Orbits

1. Introduction

Approximately 26,000 images were produced by the narrow angle camera (NAC) of the Cassini Imaging Science Subsystem (ISS) during the Cassini spacecraft's Jupiter flyby of late 2000/early 2001, providing a substantial new source of data for the study of the dynamics of the jovian satellites and rings. Porco et al. (2003) independently used ISS images to measure the orbits of Metis and Adrastea, the innermost of the four inner satellites. They empirically demonstrated for the first time that the inclinations of Metis and Adrastea are consistent with the thickness of the jovian main ring, thus supporting the hypothesis that the satellites are themselves the source of the ring material (Burns et al., 1999). This has since been confirmed by Evans et al. (2005), using both Cassini and Galileo data.

The primary purpose of this paper is to make available new Cassini observations of the other two inner satellites, Amalthea and Thebe. The procedures used to reduce and process the observations are described in the main body of the paper and in Appendix A. Orbital solutions are also provided, based on a precessing Keplerian ellipse model, and brief comments are included in Section 4 regarding the implications of the fitted orbital elements, in view of current knowledge of the geometric relationship between the inner satellites and the ring system. A more in-depth examination of these issues is beyond the scope of this paper, and the reader is referred to Porco et al. (2003) and Evans et al. (2005) for further discussion.

The timing of this work was partly dictated by JPL's need for new observations of Amalthea, to help in the planning of the close encounter between the Galileo spacecraft and Amalthea scheduled for November 2002. Cassini observations of Amalthea proved to be important both because of their better accuracy than existing Earth-based data and due to the lack

* Corresponding author. Fax: +44 (0) 20 8983 3522.
E-mail address: n.cooper@qmul.ac.uk (N.J. Cooper).

0019-1035/$ – see front matter
doi:10.1016/j.icarus.2005.11.007

of Galileo optical navigation data for this encounter (Jacobson, R.A., personal communication). Observations of Thebe were made subsequently from the same pool of images used to measure Amalthea. Thus, it should perhaps be emphasised that this work does not by any means represent an exhaustive search for all possible observations of these satellites within the entire Cassini ISS data set.

2. Satellite astrometry

Image re-pointing and satellite measurements were made using IDL-based procedures within the framework of the MINAS (Modular Image Navigation and Analysis Software) package, developed at Cassini Imaging Central Laboratory for Operations (CICLOPS). Before describing these particular procedures, we firstly outline the technique used to select images for measurement.

2.1. Image search

Given the large number of available images, an automatic FORTRAN-based search procedure was developed in order to identify images worthy of actual visual inspection. Routines from the SPICE library (Acton, 1996) were used. Timing information extracted from the image headers was combined with positions obtained from published JPL ephemerides and raw C-kernels (containing approximate camera pointing information). Using this information, it was then possible to determine automatically those images which were likely to contain the required satellites. Since most of the NAC observations were targeted directly at Jupiter, and covered more than one Jupiter diameter, Amalthea and Thebe were within the field-of-view, serendipitously, for more than 40% of the total number of NAC images (excluding those in which they were occulted by Jupiter). However, detection was possible only in the comparatively small subset of these observations which were designed specifically for the imaging of the small inner satellites and faint rings (Throop et al., 2004): in this work, we have used the 'ring movie' image sequences.

Two 'ring movie' sequences were collected during the Jupiter flyby, one on the approach to Jupiter (sequence ISS_C23RI_RMOV000_PRIME_RING), at low phase angles (less than 2°) and one on the outbound leg (sequence ISS_C24RI_RMOVOUT000_PRIME_RING), with the cameras pointed back towards Jupiter, giving phase angles of up to 122°. Based on the preliminary search analysis, approximately 500 of the 'ring movie' images were targeted for further study.

Some Cassini ISS images are binned, in order to improve the signal-to-noise ratio, by summing adjacent pixels, either 2-by-2 (producing 512-by-512 pixel images) or 4-by-4 (producing 256-by-256 pixel images). The selected images included a mixture of 'standard' size 1024-by-1024 pixel images, 2-by-2 summed and 4-by-4 summed images.

Throughout the text, we describe the measured coordinates of each satellite in a given image in terms of 'line' and 'sample,' which are equivalent to 'row' and 'column.' The origin of the *line* and *sample* coordinate system is at the centre of the top left pixel, with *line* increasing downwards and *sample* to the right, when the image is displayed in its normal orientation. The spacecraft $-X$ axis points in the direction of increasing *line* and $-Z$ axes in the increasing *sample* direction. See Porco et al. (2004) for further details on the Cassini Imaging Science Subsystem.

The inbound and outbound series of images have frame numbers beginning with N1355 and N1358, respectively, and will be referred to using these prefixes.

2.2. Image re-pointing

Approximate camera pointing information for each image was extracted from binary C-kernels, in the form of a 3-by-3 rotation matrix (C-matrix). This approximate camera pointing direction was then adjusted by comparing the estimated positions of suitable reference objects with their actual imaged positions, in order to derive a pointing correction. The correction procedure is described in more detail below. In the selected image sequences, background stars were the only suitable reference objects from which to derive such a correction. The Galilean satellites Io and Europa were occasionally present, but the high exposure levels necessary to resolve the small inner satellites made the limbs of the Galileans difficult to locate with confidence. Also, the disc of Jupiter was outside the field-of-view in most of the selected 'ring movie' images, since these sequences were specifically designed in order to view the faint ring system.

In order to derive the pointing correction for each image, reference star positions were extracted from the Hubble Space Telescope Guide Star Catalog (version GSC 2.2). Stars were chosen based on their residuals resulting from the iterative fitting process, described below, and their area distribution within a given image. The number of stars used for each image ranged from 2 to 52, with a mean of 12. Magnitudes of chosen stars were typically in the range 13 to 15.

The manual pointing correction scheme available in MINAS was compared with a new procedure, also IDL-based, which allowed images to be re-pointed automatically. In the automatic approach, MINAS routines were firstly used to compute the line and sample positions for both the raw star field (based on the uncorrected camera pointing) and the star field scanned from the image (corresponding to the 'correct' star locations). Synthetic images were then generated for each of the two star fields, by placing a unit amplitude spike at each star position and then convolving the resulting 'spiky images' with a Gaussian point-spread function. The two resulting synthetic images were then 2D cross-correlated in the frequency domain, by performing a 2D FFT of each image, then multiplying the 2D FFT of one image by the complex conjugate of the 2D FFT of the other. The inverse 2D FFT of the result produces the 2D cross-correlation function, and the line and sample coordinates of the maximum of this function then correspond to the translation in line and sample between the two star fields, representing the required gross pointing correction. The frequency domain implementation of 2D cross-correlation, described above, was found to be two orders of magnitude faster than the equivalent operation

performed directly in the line/sample domain, taking approximately 10 s per image on a modest-sized desktop PC. Following the automatic re-pointing step, a statistical fit was performed, as before, using MINAS, solving for any residual translation and rotation.

Fully automatic re-pointing was possible for all but three of the 116 selected N1358-series images, while in contrast, none of the N1355-series images could be re-pointed automatically, due to the poorer quality of reference star signals in these images. Exposure lengths were generally longer for the selected N1358 images (either 5.6 or 8.2 s) compared to the N1355 series (0.56, 1.0, 2.0, or 2.6 s). The manual re-pointing method, which is less sensitive to the signal-to-noise ratio, was therefore preferred for the N1355 images.

After correction, the final RMS pointing errors, averaged over all images, were 0.0723 lines and 0.0722 samples. In each case, this is an order of magnitude smaller than the RMS error obtained for the fitted orbital solution (Section 3), thus indicating the success of the re-pointing procedure overall.

Pointing information for each image is given in Table 1, in terms of α, δ, and ϕ. These are the nominal right ascension, declination and twist angles, respectively, for the camera optical axis, relative to the International Celestial Reference Frame (ICRF). Equation (A.4) may then be used to convert the pointing information for a given image to the equivalent C-matrix.

The camera pointing for a given image is also dependent on the spacecraft position, which is encapsulated in a binary SPICE kernel, referred to as the tour kernel. The tour kernel used for this work is 010420R-SCPSE-EP1-JP83.bsp (Table 2), which is available from ftp://naif.jpl.nasa.gov/pub/naif/. It is essential that the pointing information described in Table 1 is used with this particular tour kernel. If a different tour kernel is to be used, the pointing corrections must be re-estimated. For those practitioners who wish to re-estimate the pointing, either using a different tour kernel or star catalog, the measured line and sample positions for the reference stars for each image may be obtained in electronic form from the corresponding author, on request.

2.3. Satellite measurement

The satellites of interest were not resolved in the chosen images and hence a centroiding technique was used in order to measure line and sample locations at the sub-pixel level, corresponding to the 'centre-of-light' of each satellite.

The high phase angles for the N1358 series images required an adjustment of the measured centroids to be made before orbit determination. This correction was found to be essential in order to avoid significant systematic bias. For example, based on an assumed image resolution of 100 km/pixel and taking the longest semi-axis of Amalthea, the largest of the inner jovian satellites, to be 125 km (Thomas et al., 1998), the measured centre-of-light for Amalthea could be offset from the desired centre-of-mass location by an amount of the order of 1 NAC pixel, for viewing at 180° phase.

A simple linear relationship between the apparent pixel shift, δp, in the position of the centre-of-mass of the satellite due to the phase effect, and the phase angle, ϕ was assumed, given by

$$\delta p = \frac{\phi r}{\pi \eta}, \tag{1}$$

where r is the radius of the satellite in km and η, the image resolution in km/pixel at the location of the target satellite. The computed pixel shift, δp, was then resolved into image line, $\delta l = \delta p \sin\alpha$, and sample, $\delta s = \delta p \cos\alpha$ components, where the angle α is given by

$$\alpha = \tan^{-1}\left(\frac{l_{\text{sun}} - l_{\text{sat}}}{s_{\text{sun}} - s_{\text{sat}}}\right) \tag{2}$$

and $(l_{\text{sun}}, s_{\text{sun}})$ and $(l_{\text{sat}}, s_{\text{sat}})$ are the image coordinates of the Sun and satellite, respectively. The phase angle, ϕ, in radians, was estimated using SPICE routines *subsol* and *illum*, given the inertial positions of the Sun, spacecraft and target (extracted from the appropriate JPL ephemerides).

The computed phase corrections for the inbound N1355 series were negligible in comparison to the outbound N1358 sequence, owing to the much smaller inbound phase angles (typically 2° or less, compared to up to 122°). On the other hand, for frame N1358333008, typical of the outbound N1358 sequence, the centroid of Amalthea moved by −0.491 lines and 0.12 samples after phase correction. The correction was also generally much larger in the line direction than the sample direction for the N1358 image series, since the orientation of the spacecraft in these images was such that the ecliptic was approximately parallel to the line axis. Phase-dependent effects were therefore correspondingly larger in this direction.

Scattered light from Jupiter resulted in a significant background noise gradient in the majority of images, with the potential to bias measured centroid positions. A subtractive median filtering technique was found to be effective in removing the noise gradient, however, tests showed the effects of the noise on the measured centroid positions to be insignificant, since the limited lateral extent of the imaged satellite signals meant that the noise gradient across a given satellite signal was negligible. Thus scattered light removal was deemed to be unnecessary.

We provide the raw measured line and sample values for each satellite in Table 1. Line and sample values are given with respect to actual image sizes. Phase correction (as described above) has not been applied to the tabulated values. Phase-corrected values may be obtained from the corresponding author in electronic form, if required. In Appendix A, we describe how a model-derived Cartesian position vector in the planetocentric frame may be converted to equivalent line and sample values, using the derived pointing information from Table 1, thus allowing equations of condition to be developed for orbit fitting purposes. We choose to provide the observations and pointing information in their raw form in Table 1 in order to allow the user to modify the pointing and/or phase correction, if so desired. For example, the non-linear camera distortion parameters provided in Table 3 are based on JPL's April 2003 analysis (Owen, 2003). Updated model parameters may be made available by JPL as the Cassini mission proceeds.

The longitude coverage for the complete set of observations is shown in Fig. 1. Observations of Amalthea include segments from seven different orbits (three from the N1355 image

Table 1
Cassini ISS NAC observations

Frame	Image mid-time (UTC)	Size	RA[a] (deg)	Dec (deg)	Twist (deg)	Sample[b]	Line	Object
n1355254240	2000 DEC 11 19:19:12.520	512	63.626184	19.962424	190.252894	497.90	220.00	Amalthea
n1355254579	2000 DEC 11 19:24:52.538	512	63.631766	19.963856	190.386255	467.96	221.14	Amalthea
…	…	…	…	…	…	13.03	276.81	Thebe
n1355254739	2000 DEC 11 19:27:31.817	512	63.634381	19.964417	190.405306	454.22	222.00	Amalthea
…	…	…	…	…	…	14.16	277.93	Thebe
n1355255239	2000 DEC 11 19:35:52.533	512	63.643123	19.966043	190.343183	413.83	223.80	Amalthea
…	…	…	…	…	…	20.23	280.93	Thebe
n1355255560	2000 DEC 11 19:41:12.511	512	63.648871	19.967179	190.460537	389.21	225.03	Amalthea
n1355257043	2000 DEC 11 20:05:56.540	512	63.677396	19.972548	190.369067	294.98	231.92	Amalthea
…	…	…	…	…	…	68.25	292.02	Thebe
n1355257205	2000 DEC 11 20:08:37.800	512	63.678905	19.973234	190.355635	283.94	233.16	Amalthea
…	…	…	…	…	…	72.00	293.77	Thebe
n1355257705	2000 DEC 11 20:16:58.516	512	63.685728	19.974566	190.431472	255.84	235.88	Amalthea
n1355257865	2000 DEC 11 20:19:37.795	512	63.688489	19.975237	190.411153	248.15	236.82	Amalthea
n1355258026	2000 DEC 11 20:22:18.494	512	63.691466	19.975490	190.434353	241.20	237.06	Amalthea
…	…	…	…	…	…	101.98	297.87	Thebe
n1355258365	2000 DEC 11 20:27:58.512	512	63.697506	19.976822	190.316041	227.30	239.18	Amalthea
…	…	…	…	…	…	117.12	299.94	Thebe
n1355258525	2000 DEC 11 20:30:37.790	512	63.700165	19.977411	190.407175	221.78	239.99	Amalthea
n1355258686	2000 DEC 11 20:33:18.489	512	63.702915	19.977901	190.325751	216.10	240.95	Amalthea
n1355259025	2000 DEC 11 20:38:58.507	512	63.709083	19.979015	190.345468	205.32	242.93	Amalthea
…	…	…	…	…	…	150.06	303.02	Thebe
n1355259185	2000 DEC 11 20:41:37.786	512	63.711822	19.979482	190.330297	201.12	243.80	Amalthea
…	…	…	…	…	…	158.80	303.87	Thebe
n1355259346	2000 DEC 11 20:44:18.485	512	63.714524	19.979712	190.343088	196.84	244.09	Amalthea
…	…	…	…	…	…	166.97	304.01	Thebe
n1355260829	2000 DEC 11 21:09:02.514	512	63.737519	19.984485	190.365772	175.17	253.27	Amalthea
…	…	…	…	…	…	254.95	310.96	Thebe
n1355260991	2000 DEC 11 21:11:43.773	512	63.740284	19.984449	190.400523	174.98	253.90	Amalthea
n1355261152	2000 DEC 11 21:14:24.472	512	63.742824	19.985524	190.367337	175.76	255.03	Amalthea
…	…	…	…	…	…	276.83	311.89	Thebe
n1355261491	2000 DEC 11 21:20:04.490	512	63.748556	19.986679	190.416314	177.73	257.74	Amalthea
…	…	…	…	…	…	300.13	313.19	Thebe
n1355261651	2000 DEC 11 21:22:43.769	512	63.751171	19.987131	190.314609	179.21	258.08	Amalthea
…	…	…	…	…	…	311.99	313.80	Thebe
n1355261812	2000 DEC 11 21:25:24.468	512	63.754040	19.987323	190.374529	181.73	258.78	Amalthea
…	…	…	…	…	…	323.92	313.82	Thebe
n1355262151	2000 DEC 11 21:31:04.485	512	63.759924	19.989040	190.361269	187.81	261.18	Amalthea
…	…	…	…	…	…	349.90	315.14	Thebe
n1355262311	2000 DEC 11 21:33:43.764	512	63.762502	19.989543	190.336425	191.01	262.15	Amalthea
…	…	…	…	…	…	361.99	315.92	Thebe
n1355262472	2000 DEC 11 21:36:24.463	512	63.765444	19.989976	190.318556	194.78	262.94	Amalthea
n1355262811	2000 DEC 11 21:42:04.481	512	63.771004	19.991143	190.322248	204.06	265.10	Amalthea
…	…	…	…	…	…	401.21	317.06	Thebe
n1355262971	2000 DEC 11 21:44:43.760	512	63.773864	19.991491	190.355055	209.27	265.88	Amalthea
…	…	…	…	…	…	414.89	317.11	Thebe
n1355263132	2000 DEC 11 21:47:24.459	512	63.776374	19.991916	190.327144	214.81	266.82	Amalthea
n1355264615	2000 DEC 11 22:12:08.488	512	63.801625	19.996973	190.381381	283.99	274.94	Amalthea
n1355264777	2000 DEC 11 22:14:49.747	512	63.804176	19.997549	190.295240	293.08	275.84	Amalthea
n1355264938	2000 DEC 11 22:17:30.446	512	63.807283	19.997804	190.400225	303.05	276.16	Amalthea
n1355265277	2000 DEC 11 22:23:10.464	512	63.812978	19.999514	190.314968	325.21	278.28	Amalthea
n1355265437	2000 DEC 11 22:25:49.743	512	63.815914	19.999857	190.327439	336.06	279.08	Amalthea
n1355265598	2000 DEC 11 22:28:30.442	512	63.818666	19.999926	190.336353	347.04	279.26	Amalthea
n1355265937	2000 DEC 11 22:34:10.459	512	63.824088	20.001464	190.310152	371.73	281.22	Amalthea
n1355266097	2000 DEC 11 22:36:49.738	512	63.826787	20.001967	190.251195	383.87	281.90	Amalthea
n1355266258	2000 DEC 11 22:39:30.437	512	63.829705	20.001874	190.359186	396.08	282.12	Amalthea
n1355266757	2000 DEC 11 22:47:49.733	512	63.838139	20.004101	190.302708	436.91	284.92	Amalthea
n1355266918	2000 DEC 11 22:50:30.432	512	63.841050	20.004356	190.320383	450.92	284.98	Amalthea
n1355298689	2000 DEC 12 07:40:02.252	512	64.387843	20.109278	189.983086	379.31	225.10	Amalthea
n1355299012	2000 DEC 12 07:45:24.210	512	64.393077	20.110501	190.210154	354.96	226.23	Amalthea
n1355299351	2000 DEC 12 07:51:04.228	512	64.399119	20.111743	189.987039	330.30	227.98	Amalthea
n1355299511	2000 DEC 12 07:53:43.507	512	64.401816	20.112095	190.086855	319.78	228.84	Amalthea

(*continued on the next page*)

Table 1 (*continued*)

Frame	Image mid-time (UTC)	Size	RA[a] (deg)	Dec (deg)	Twist (deg)	Sample[b]	Line	Object
n1355299672	2000 DEC 12 07:56:24.206	512	64.404555	20.112634	190.045431	308.92	229.16	Amalthea
n1355300011	2000 DEC 12 08:02:04.223	512	64.410984	20.113628	190.016496	287.35	230.97	Amalthea
n1355300171	2000 DEC 12 08:04:43.502	512	64.413776	20.114515	190.080860	278.15	232.02	Amalthea
n1355300332	2000 DEC 12 08:07:24.201	512	64.416804	20.114807	190.089235	269.03	232.24	Amalthea
n1355300671	2000 DEC 12 08:13:04.219	512	64.422898	20.116179	190.074534	250.93	234.29	Amalthea
n1355300831	2000 DEC 12 08:15:43.498	512	64.425693	20.116778	190.051224	242.86	235.27	Amalthea
n1355302475	2000 DEC 12 08:43:08.226	512	64.453261	20.121424	190.026918	179.13	243.83	Amalthea
…	…	…	…	…	…	474.83	207.10	Thebe
n1355302637	2000 DEC 12 08:45:49.485	512	64.455503	20.122064	190.080594	174.77	245.15	Amalthea
n1355302798	2000 DEC 12 08:48:30.184	512	64.458373	20.122429	190.085454	171.16	245.93	Amalthea
…	…	…	…	…	…	445.22	209.06	Thebe
n1355303137	2000 DEC 12 08:54:10.202	512	64.464520	20.123989	190.029687	165.29	248.12	Amalthea
…	…	…	…	…	…	416.05	211.12	Thebe
n1355303297	2000 DEC 12 08:56:49.480	512	64.467254	20.124201	190.060870	163.24	248.93	Amalthea
…	…	…	…	…	…	402.82	211.96	Thebe
n1355303458	2000 DEC 12 08:59:30.179	512	64.470324	20.124888	190.039713	161.97	249.95	Amalthea
…	…	…	…	…	…	389.13	212.93	Thebe
n1355303797	2000 DEC 12 09:05:10.197	512	64.476389	20.126066	190.036427	159.97	252.11	Amalthea
…	…	…	…	…	…	361.78	214.99	Thebe
n1355303957	2000 DEC 12 09:07:49.476	512	64.479001	20.126689	190.023612	159.21	253.12	Amalthea
…	…	…	…	…	…	348.23	215.99	Thebe
n1355304118	2000 DEC 12 09:10:30.175	512	64.482488	20.126870	190.003700	160.04	253.74	Amalthea
…	…	…	…	…	…	336.16	216.11	Thebe
n1355304457	2000 DEC 12 09:16:10.192	512	64.488222	20.128321	190.055809	161.20	256.16	Amalthea
…	…	…	…	…	…	309.86	218.99	Thebe
n1355304617	2000 DEC 12 09:18:49.471	512	64.490938	20.128950	190.037355	162.84	257.11	Amalthea
…	…	…	…	…	…	297.83	219.95	Thebe
n1355304778	2000 DEC 12 09:21:30.170	512	64.494090	20.129475	190.012467	164.84	258.02	Amalthea
…	…	…	…	…	…	285.93	220.89	Thebe
n1355306261	2000 DEC 12 09:46:14.199	512	64.521101	20.134723	190.022321	201.99	267.00	Amalthea
…	…	…	…	…	…	185.50	230.50	Thebe
n1355306423	2000 DEC 12 09:48:55.459	512	64.524479	20.135073	190.024824	208.82	267.85	Amalthea
…	…	…	…	…	…	176.09	231.16	Thebe
n1355306584	2000 DEC 12 09:51:36.158	512	64.527348	20.135435	190.037343	215.19	268.18	Amalthea
…	…	…	…	…	…	166.90	232.03	Thebe
n1355306923	2000 DEC 12 09:57:16.175	512	64.533603	20.136776	190.011543	230.29	270.80	Amalthea
…	…	…	…	…	…	147.19	234.92	Thebe
n1355307083	2000 DEC 12 09:59:55.454	512	64.536724	20.137458	189.957919	238.02	271.77	Amalthea
…	…	…	…	…	…	138.50	235.99	Thebe
n1355307244	2000 DEC 12 10:02:36.153	512	64.539258	20.137757	190.022584	245.97	272.18	Amalthea
…	…	…	…	…	…	129.86	236.96	Thebe
n1355307583	2000 DEC 12 10:08:16.171	512	64.544871	20.139107	190.032363	263.86	274.19	Amalthea
…	…	…	…	…	…	111.50	239.50	Thebe
n1355307743	2000 DEC 12 10:10:55.450	512	64.547327	20.139461	190.020881	272.23	275.11	Amalthea
…	…	…	…	…	…	103.11	240.78	Thebe
n1355307904	2000 DEC 12 10:13:36.149	512	64.550389	20.140208	189.839640	281.74	275.88	Amalthea
n1355308243	2000 DEC 12 10:19:16.166	512	64.555677	20.141161	190.032364	302.89	277.89	Amalthea
…	…	…	…	…	…	79.78	244.07	Thebe
n1355308403	2000 DEC 12 10:21:55.445	512	64.558447	20.141538	190.018434	313.16	278.23	Amalthea
…	…	…	…	…	…	72.79	245.04	Thebe
n1355308564	2000 DEC 12 10:24:36.144	512	64.561260	20.141977	190.004514	324.05	279.01	Amalthea
…	…	…	…	…	…	65.87	246.02	Thebe
n1355310209	2000 DEC 12 10:52:01.433	512	64.591594	20.147719	189.963600	457.05	286.13	Amalthea
…	…	…	…	…	…	14.23	257.95	Thebe
n1355340497	2000 DEC 12 19:16:49.223	512	65.134706	20.249651	189.799086	483.17	219.20	Amalthea
n1355340658	2000 DEC 12 19:19:29.922	512	65.137659	20.250138	189.755032	468.30	219.97	Amalthea
n1355340997	2000 DEC 12 19:25:09.939	512	65.143532	20.251197	189.796627	437.79	221.08	Amalthea
n1355341157	2000 DEC 12 19:27:49.218	512	65.146294	20.251521	189.774176	423.78	221.18	Amalthea
n1355341318	2000 DEC 12 19:30:29.917	512	65.149221	20.252232	189.823791	409.95	222.05	Amalthea
n1355341657	2000 DEC 12 19:36:09.935	512	65.155696	20.253461	189.813961	381.95	223.85	Amalthea
n1355341817	2000 DEC 12 19:38:49.214	512	65.158618	20.253772	189.786520	369.16	224.17	Amalthea
n1355341978	2000 DEC 12 19:41:29.913	512	65.162014	20.254214	189.745698	357.06	224.26	Amalthea
n1355342317	2000 DEC 12 19:47:09.930	512	65.167883	20.255801	189.782595	331.20	226.84	Amalthea

(*continued on the next page*)

Table 1 (*continued*)

Frame	Image mid-time (UTC)	Size	RA[a] (deg)	Dec (deg)	Twist (deg)	Sample[b]	Line	Object
n1355342477	2000 DEC 12 19:49:49.209	512	65.170835	20.256154	189.797576	319.83	227.04	Amalthea
n1355342638	2000 DEC 12 19:52:29.908	512	65.173259	20.256439	189.737338	307.87	227.83	Amalthea
n1355344121	2000 DEC 12 20:17:13.937	512	65.198898	20.261534	189.782465	218.06	235.84	Amalthea
n1355344191	2000 DEC 12 20:18:23.697	256	65.200269	20.261476	189.831659	106.99	117.93	Amalthea
n1355344444	2000 DEC 12 20:22:35.896	512	65.204241	20.261947	189.782053	202.83	236.95	Amalthea
n1355344783	2000 DEC 12 20:28:15.913	512	65.210570	20.263529	189.790561	188.84	239.17	Amalthea
n1355344851	2000 DEC 12 20:29:23.693	256	65.211768	20.264079	189.545283	92.97	119.75	Amalthea
n1355344943	2000 DEC 12 20:30:55.192	512	65.213591	20.264027	189.792685	183.03	240.17	Amalthea
n1355345104	2000 DEC 12 20:33:35.891	512	65.216802	20.264471	189.793271	177.73	240.89	Amalthea
n1355345443	2000 DEC 12 20:39:15.909	512	65.222639	20.265503	189.827732	166.39	242.95	Amalthea
n1355345603	2000 DEC 12 20:41:55.187	512	65.225747	20.266235	189.765477	162.33	243.98	Amalthea
n1355345764	2000 DEC 12 20:44:35.886	512	65.228776	20.266532	189.815997	158.98	244.85	Amalthea
n1355346103	2000 DEC 12 20:50:15.904	512	65.234829	20.268074	189.762896	151.34	247.08	Amalthea
n1355346171	2000 DEC 12 20:51:23.684	256	65.236251	20.268245	189.924710	75.04	123.74	Amalthea
n1355346263	2000 DEC 12 20:52:55.183	512	65.237723	20.268552	189.765286	149.02	248.01	Amalthea
n1355346424	2000 DEC 12 20:55:35.882	512	65.240547	20.268942	189.768654	146.79	248.85	Amalthea
n1355347907	2000 DEC 12 21:20:19.911	512	65.268105	20.274176	189.792901	147.29	258.14	Amalthea
n1355347977	2000 DEC 12 21:21:29.671	256	65.269353	20.273965	189.975624	73.92	129.03	Amalthea
n1355348069	2000 DEC 12 21:23:01.170	512	65.270993	20.274571	189.739516	149.23	258.86	Amalthea
n1355348230	2000 DEC 12 21:25:41.869	512	65.273864	20.275249	189.733860	152.03	259.97	Amalthea
n1355348569	2000 DEC 12 21:31:21.887	512	65.279624	20.276157	189.790272	158.33	262.10	Amalthea
n1355348729	2000 DEC 12 21:34:01.166	512	65.283147	20.276749	189.741711	162.91	263.00	Amalthea
n1355348890	2000 DEC 12 21:36:41.865	512	65.286160	20.277093	189.752003	167.22	263.26	Amalthea
n1355349229	2000 DEC 12 21:42:21.882	512	65.291855	20.278647	189.802868	177.83	266.18	Amalthea
n1355349389	2000 DEC 12 21:45:01.161	512	65.295050	20.279147	189.769018	183.22	266.96	Amalthea
n1355349550	2000 DEC 12 21:47:41.860	512	65.298166	20.279616	189.774352	190.00	267.96	Amalthea
n1355349889	2000 DEC 12 21:53:21.878	512	65.304722	20.280995	189.753063	204.39	270.01	Amalthea
n1355349957	2000 DEC 12 21:54:29.657	256	65.306643	20.281497	189.603660	103.86	134.99	Amalthea
n1355350049	2000 DEC 12 21:56:01.157	512	65.308072	20.281371	189.788302	212.25	270.89	Amalthea
n1355350210	2000 DEC 12 21:58:41.856	512	65.310894	20.281859	189.737696	220.05	271.87	Amalthea
n1355351693	2000 DEC 12 22:23:25.885	512	65.337662	20.287106	189.616109	309.08	279.29	Amalthea
n1355351763	2000 DEC 12 22:24:35.645	256	65.338904	20.287401	189.758564	156.92	139.77	Amalthea
n1355351855	2000 DEC 12 22:26:07.144	512	65.340313	20.287495	189.636478	320.23	280.24	Amalthea
n1355352016	2000 DEC 12 22:28:47.843	512	65.343464	20.287996	189.609481	332.74	281.00	Amalthea
n1355352355	2000 DEC 12 22:34:27.861	512	65.350035	20.289384	189.717628	359.25	282.82	Amalthea
n1355352515	2000 DEC 12 22:37:07.140	512	65.352979	20.290012	189.652601	372.09	283.75	Amalthea
n1355353015	2000 DEC 12 22:45:27.856	512	65.362535	20.291625	189.767983	414.98	285.31	Amalthea
n1355353175	2000 DEC 12 22:48:07.135	512	65.365590	20.292406	189.666849	429.26	286.29	Amalthea
n1355353675	2000 DEC 12 22:56:27.852	512	65.374593	20.293808	189.714657	475.13	288.04	Amalthea
n1355353835	2000 DEC 12 22:59:07.130	512	65.377807	20.294542	189.708438	490.81	288.91	Amalthea
n1358243728	2001 JAN 15 09:43:38.318	512	190.035259	−2.195363	245.101420	273.97	350.89	Amalthea
n1358243908	2001 JAN 15 09:46:37.017	512	190.038618	−2.196151	245.053350	273.18	356.92	Amalthea
n1358244088	2001 JAN 15 09:49:37.015	1024	190.041538	−2.199046	245.123141	541.09	724.79	Amalthea
n1358244268	2001 JAN 15 09:52:38.314	512	190.044895	−2.200309	245.152299	269.22	367.03	Amalthea
n1358244448	2001 JAN 15 09:55:37.013	512	190.048128	−2.201510	245.132044	268.94	371.82	Amalthea
n1358244628	2001 JAN 15 09:58:37.012	1024	190.051681	−2.202632	245.116057	536.91	750.92	Amalthea
n1358244808	2001 JAN 15 10:01:38.310	512	190.054566	−2.204808	245.097801	265.82	378.80	Amalthea
n1358244988	2001 JAN 15 10:04:37.009	512	190.057918	−2.206286	245.114687	264.22	381.05	Amalthea
n1358245168	2001 JAN 15 10:07:37.008	1024	190.061613	−2.207382	245.104716	528.85	766.62	Amalthea
n1358246208	2001 JAN 15 10:24:58.301	512	190.080555	−2.215456	245.107837	257.88	383.88	Amalthea
n1358246388	2001 JAN 15 10:27:57.000	512	190.083531	−2.217444	245.112883	255.21	381.96	Amalthea
n1358246568	2001 JAN 15 10:30:56.998	1024	190.087138	−2.218883	245.132284	509.82	758.89	Amalthea
n1358246748	2001 JAN 15 10:33:58.297	512	190.090588	−2.219518	245.094995	254.16	376.24	Amalthea
n1358246928	2001 JAN 15 10:36:56.996	512	190.094059	−2.220565	245.090674	253.88	372.93	Amalthea
n1358247108	2001 JAN 15 10:39:56.995	1024	190.096974	−2.222863	245.122000	503.11	737.87	Amalthea
n1358247288	2001 JAN 15 10:42:58.293	512	190.100398	−2.224211	245.098892	250.14	363.90	Amalthea
n1358247468	2001 JAN 15 10:45:56.992	512	190.103951	−2.225139	245.096502	250.00	358.27	Amalthea
n1358247648	2001 JAN 15 10:48:56.991	1024	190.107367	−2.226191	245.099181	499.10	705.89	Amalthea
n1358248688	2001 JAN 15 11:06:18.284	512	190.126193	−2.235085	245.114955	241.96	307.90	Amalthea
n1358248868	2001 JAN 15 11:09:16.982	512	190.129641	−2.235962	245.103664	241.30	298.04	Amalthea
n1358249048	2001 JAN 15 11:12:16.981	1024	190.133181	−2.236972	245.118084	482.82	576.90	Amalthea
n1358249228	2001 JAN 15 11:15:18.280	512	190.136780	−2.237984	245.089956	240.94	277.71	Amalthea
n1358249408	2001 JAN 15 11:18:16.979	512	190.139733	−2.240255	245.081390	238.11	266.12	Amalthea

(*continued on the next page*)

Table 1 (*continued*)

Frame	Image mid-time (UTC)	Size	RA[a] (deg)	Dec (deg)	Twist (deg)	Sample[b]	Line	Object
n1358249588	2001 JAN 15 11:21:16.977	1024	190.142886	−2.241408	245.121907	475.74	510.73	Amalthea
n1358249768	2001 JAN 15 11:24:18.276	512	190.146658	−2.242757	245.070978	236.90	242.47	Amalthea
n1358250128	2001 JAN 15 11:30:16.974	1024	190.152814	−2.245551	245.133539	469.86	434.76	Amalthea
n1358251168	2001 JAN 15 11:47:38.266	512	190.172327	−2.253244	245.148742	230.04	132.33	Amalthea
n1358251528	2001 JAN 15 11:53:36.964	1024	190.179066	−2.255425	245.142642	458.79	200.15	Amalthea
n1358251708	2001 JAN 15 11:56:38.263	512	190.182197	−2.257663	245.163123	226.21	82.55	Amalthea
…	…	…	…	…	…	208.04	436.90	Thebe
n1358283588	2001 JAN 15 20:47:56.742	512	190.757983	−2.500732	245.195769	289.05	137.20	Amalthea
n1358283768	2001 JAN 15 20:50:56.741	1024	190.760472	−2.502521	245.183820	575.14	305.93	Amalthea
n1358283948	2001 JAN 15 20:53:58.039	512	190.764067	−2.503178	245.203954	287.89	166.76	Amalthea
n1358284128	2001 JAN 15 20:56:56.738	512	190.767600	−2.504056	245.201831	287.94	180.07	Amalthea
n1358284308	2001 JAN 15 20:59:56.737	1024	190.770647	−2.505894	245.181931	573.04	387.99	Amalthea
n1358284488	2001 JAN 15 21:02:58.036	512	190.773100	−2.508314	245.195017	283.87	206.91	Amalthea
n1358284668	2001 JAN 15 21:05:56.734	512	190.776525	−2.508913	245.192520	284.02	219.75	Amalthea
n1358284848	2001 JAN 15 21:08:56.733	1024	190.780383	−2.509654	245.194989	569.27	463.10	Amalthea
n1358285888	2001 JAN 15 21:26:18.026	512	190.798610	−2.517703	245.199220	278.97	291.95	Amalthea
n1358286068	2001 JAN 15 21:29:16.725	512	190.801174	−2.519724	245.187194	276.78	300.90	Amalthea
n1358286248	2001 JAN 15 21:32:16.724	1024	190.804595	−2.520749	245.187963	552.95	618.87	Amalthea
n1358286428	2001 JAN 15 21:35:18.022	512	190.808348	−2.521920	245.184865	275.88	316.14	Amalthea
n1358286608	2001 JAN 15 21:38:16.721	512	190.811507	−2.522672	245.166334	275.74	323.83	Amalthea
n1358286788	2001 JAN 15 21:41:16.720	1024	190.814203	−2.524964	245.194837	546.82	661.77	Amalthea
n1358286968	2001 JAN 15 21:44:18.019	512	190.817014	−2.526687	245.191569	271.11	336.96	Amalthea
n1358287148	2001 JAN 15 21:47:16.717	512	190.820756	−2.527056	245.190649	271.94	342.16	Amalthea
n1358287328	2001 JAN 15 21:50:16.716	1024	190.824431	−2.528073	245.201527	543.92	694.81	Amalthea
n1358288368	2001 JAN 15 22:07:38.009	512	190.842408	−2.536563	245.179448	264.06	365.74	Amalthea
n1358288548	2001 JAN 15 22:10:36.708	512	190.845411	−2.538253	245.180142	262.75	366.93	Amalthea
n1358288728	2001 JAN 15 22:13:36.706	1024	190.848697	−2.539257	245.186378	524.77	735.85	Amalthea
n1358288908	2001 JAN 15 22:16:38.005	512	190.852634	−2.539943	245.144609	262.13	367.06	Amalthea
n1358289088	2001 JAN 15 22:19:36.704	512	190.855365	−2.541380	245.186320	260.96	367.11	Amalthea
n1358289268	2001 JAN 15 22:22:36.703	1024	190.858007	−2.543658	245.195444	516.83	733.59	Amalthea
n1358289448	2001 JAN 15 22:25:38.001	512	190.861067	−2.545392	245.172957	256.18	364.92	Amalthea
n1358289628	2001 JAN 15 22:28:36.700	512	190.864545	−2.545796	245.209972	256.88	362.89	Amalthea
n1358289808	2001 JAN 15 22:31:36.699	1024	190.868131	−2.546738	245.205040	513.10	720.01	Amalthea
n1358290848	2001 JAN 15 22:48:57.992	512	190.886125	−2.555179	245.173587	248.86	333.23	Amalthea
n1358291028	2001 JAN 15 22:51:56.690	512	190.889329	−2.556343	245.180757	247.94	326.97	Amalthea
n1358291208	2001 JAN 15 22:54:56.689	1024	190.893154	−2.556614	245.189110	497.85	640.00	Amalthea
n1358291388	2001 JAN 15 22:57:57.988	512	190.896468	−2.557263	245.244670	248.14	312.04	Amalthea
n1358291568	2001 JAN 15 23:00:56.687	512	190.899362	−2.559342	245.178414	246.17	304.11	Amalthea
n1358291748	2001 JAN 15 23:03:56.685	1024	190.902365	−2.561708	245.204742	487.99	591.05	Amalthea
n1358291928	2001 JAN 15 23:06:57.984	512	190.905435	−2.562938	245.203632	242.97	286.20	Amalthea
n1358292108	2001 JAN 15 23:09:56.683	512	190.909269	−2.562808	245.180334	243.97	276.85	Amalthea
n1358292288	2001 JAN 15 23:12:56.682	1024	190.912398	−2.564246	245.200520	486.03	533.76	Amalthea
n1358293688	2001 JAN 15 23:36:16.672	1024	190.936400	−2.575779	245.190549	466.89	342.66	Amalthea
n1358293868	2001 JAN 15 23:39:17.971	512	190.939684	−2.576812	245.197833	232.67	156.70	Amalthea
n1358294048	2001 JAN 15 23:42:16.670	512	190.942462	−2.579027	245.187412	229.83	142.53	Amalthea
n1358294228	2001 JAN 15 23:45:16.668	1024	190.945263	−2.581027	245.188585	457.17	254.83	Amalthea
n1358294768	2001 JAN 15 23:54:16.665	1024	190.955568	−2.583128	245.206587	458.01	158.94	Amalthea
n1358326108	2001 JAN 16 08:36:37.747	512	191.497995	−2.810222	245.255817	294.16	74.06	Amalthea
n1358326468	2001 JAN 16 08:42:36.445	1024	191.504419	−2.812594	245.278858	587.01	209.95	Amalthea
n1358326828	2001 JAN 16 08:48:36.443	512	191.510585	−2.814924	245.268214	292.19	134.14	Amalthea
n1358327008	2001 JAN 16 08:51:36.441	1024	191.512842	−2.817651	245.268094	578.94	297.88	Amalthea
n1358328048	2001 JAN 16 09:08:57.734	512	191.531599	−2.823743	245.275387	287.05	221.77	Amalthea
n1358328228	2001 JAN 16 09:11:56.433	512	191.535146	−2.823953	245.272123	288.00	232.83	Amalthea
n1358328408	2001 JAN 16 09:14:56.432	1024	191.538349	−2.824920	245.266699	575.92	487.60	Amalthea
n1358328588	2001 JAN 16 09:17:57.730	512	191.540664	−2.827449	245.259815	284.89	254.03	Amalthea
n1358328768	2001 JAN 16 09:20:56.429	512	191.543664	−2.829719	245.280728	282.72	263.15	Amalthea
n1358328948	2001 JAN 16 09:23:56.428	1024	191.546977	−2.830022	245.256171	566.74	545.94	Amalthea
n1358329128	2001 JAN 16 09:26:57.727	512	191.550384	−2.830478	245.250510	283.14	281.78	Amalthea
n1358329308	2001 JAN 16 09:29:56.425	512	191.553134	−2.832283	245.247046	281.77	289.99	Amalthea
n1358329488	2001 JAN 16 09:32:56.424	1024	191.555597	−2.834509	245.265893	558.76	596.61	Amalthea
n1358330528	2001 JAN 16 09:50:17.717	512	191.573895	−2.840937	245.224918	274.98	332.81	Amalthea
n1358330708	2001 JAN 16 09:53:16.416	512	191.577647	−2.840765	245.297122	276.10	336.91	Amalthea
n1358330888	2001 JAN 16 09:56:16.414	1024	191.580689	−2.841813	245.249925	551.78	681.96	Amalthea

(*continued on the next page*)

Table 1 (*continued*)

Frame	Image mid-time (UTC)	Size	RA[a] (deg)	Dec (deg)	Twist (deg)	Sample[b]	Line	Object
n1358331068	2001 JAN 16 09:59:17.713	512	191.583421	−2.843996	245.242762	273.02	343.90	Amalthea
n1358331248	2001 JAN 16 10:02:16.412	512	191.585998	−2.846427	245.245257	270.08	346.11	Amalthea
n1358331428	2001 JAN 16 10:05:16.411	1024	191.589326	−2.847289	245.264950	540.16	696.88	Amalthea
n1358331608	2001 JAN 16 10:08:17.709	512	191.592951	−2.847341	245.213998	270.84	349.77	Amalthea
n1358331788	2001 JAN 16 10:11:16.408	512	191.595773	−2.848762	245.241025	269.14	350.91	Amalthea
n1358331968	2001 JAN 16 10:14:16.407	1024	191.598344	−2.850835	245.268039	534.19	703.09	Amalthea
n1358333008	2001 JAN 16 10:31:37.700	512	191.616020	−2.858533	245.218402	260.10	342.23	Amalthea
n1358333188	2001 JAN 16 10:34:36.398	512	191.619430	−2.858811	245.213237	260.80	339.05	Amalthea
n1358333368	2001 JAN 16 10:37:36.397	1024	191.623037	−2.859326	245.265031	522.21	670.75	Amalthea
n1358333548	2001 JAN 16 10:40:37.696	512	191.625438	−2.861413	245.275564	258.23	330.90	Amalthea
n1358333728	2001 JAN 16 10:43:36.395	512	191.628285	−2.863452	245.257097	255.97	325.81	Amalthea
n1358333908	2001 JAN 16 10:46:36.393	1024	191.631292	−2.864985	245.263639	509.89	640.69	Amalthea
n1358334088	2001 JAN 16 10:49:37.692	512	191.634879	−2.865197	245.248853	255.08	313.87	Amalthea
n1358334268	2001 JAN 16 10:52:36.391	512	191.637905	−2.866044	245.270825	254.90	307.78	Amalthea
n1358334448	2001 JAN 16 10:55:36.390	1024	191.640676	−2.868334	245.261338	504.94	600.83	Amalthea
n1358335488	2001 JAN 16 11:12:57.683	512	191.658040	−2.876065	245.253947	245.16	248.87	Amalthea
n1358335668	2001 JAN 16 11:15:56.381	512	191.661406	−2.876716	245.236043	245.26	238.06	Amalthea
n1358335848	2001 JAN 16 11:18:56.380	1024	191.664766	−2.876830	245.263423	492.98	455.58	Amalthea
n1358336028	2001 JAN 16 11:21:57.679	512	191.667829	−2.878271	245.319812	245.01	215.41	Amalthea
n1358336388	2001 JAN 16 11:27:56.376	1024	191.673449	−2.881899	245.270672	483.15	382.77	Amalthea
n1358336928	2001 JAN 16 11:36:56.373	1024	191.683113	−2.885206	245.285541	479.81	301.87	Amalthea
n1358369168	2001 JAN 16 20:34:16.149	1024	192.218436	−3.109875	245.349470	597.28	112.73	Amalthea
…	…	…	…	…	…	429.82	713.67	Thebe
n1358370208	2001 JAN 16 20:51:37.442	512	192.236064	−3.116765	245.351671	295.12	140.13	Amalthea
n1358370388	2001 JAN 16 20:54:36.141	512	192.238075	−3.119106	245.346088	292.81	153.59	Amalthea
…	…	…	…	…	…	207.96	277.77	Thebe
n1358370568	2001 JAN 16 20:57:36.140	1024	192.240604	−3.121122	245.343294	581.91	333.71	Amalthea
…	…	…	…	…	…	412.08	530.09	Thebe
n1358370748	2001 JAN 16 21:00:37.438	512	192.244158	−3.121509	245.358273	291.08	178.75	Amalthea
…	…	…	…	…	…	206.18	251.90	Thebe
n1358370928	2001 JAN 16 21:03:36.137	512	192.247286	−3.122155	245.324333	291.24	190.73	Amalthea
…	…	…	…	…	…	206.94	238.70	Thebe
n1358371108	2001 JAN 16 21:06:36.136	1024	192.250241	−3.123742	245.343454	580.93	404.93	Amalthea
…	…	…	…	…	…	411.90	450.08	Thebe
n1358371288	2001 JAN 16 21:09:37.435	512	192.252218	−3.126313	245.343366	287.01	213.87	Amalthea
…	…	…	…	…	…	202.94	211.52	Thebe
n1358371468	2001 JAN 16 21:12:36.133	512	192.255254	−3.127958	245.377776	285.89	224.10	Amalthea
n1358371648	2001 JAN 16 21:15:36.132	1024	192.258446	−3.128325	245.343347	572.92	469.81	Amalthea

Notes. 1. The origin of the image *line* and *sample* coordinate system is at the center of the top left pixel, with *line* increasing downwards and *sample* to the right, when the image is displayed in its normal orientation. The spacecraft $-X$ axis points in the direction of increasing *line* and $-Z$ axes in the increasing *sample* direction. See Porco et al. (2004) for further information.

2. The data in Table 1 may be obtained from the corresponding author in electronic form, on request. Phase-corrected line and sample values are also available.

[a] Image pointing information is given in terms of RA, DEC, and TWIST angles, which refer to the right ascension, declination (both in the International Celestial Reference Frame (ICRF)), and rotation angles, respectively, for the camera optical axis. See section 3 of Appendix A for further explanation.

[b] The tabulated line and sample values are centroided 'centre-of-light' positions, i.e., phase correction, as described in Section 2.3, has not been applied. See also note 2 above.

Table 2
Constants used in orbit determination

Jupiter	Value[a]	Units
Pole (RA, DEC)	(268.05, 64.49)	deg
GM	126686537.0	km^3/s^2
Radius	71398	km
J_2	0.014736	
J_4	−0.000587	
J_6	0.000031	
Cassini tour kernel: 010420R-SCPSE-EP1-JP83.bsp		

[a] Pole position from cpck05may2004.tpc, available from ftp://naif.jpl.nasa.gov/pub/naif/, radius and zonal harmonics from Campbell and Synnott (1985). Cassini tour kernel available from ftp://naif.jpl.nasa.gov/pub/naif/.

series and four from N1358). Thebe observations cover segments from four different orbits (two from N1355 and two from N1358, although one of the N1358 orbit segments contains only one observation).

3. Orbital solutions

Orbital elements have been derived for each satellite, based on a uniformly precessing Keplerian ellipse model (Taylor, 1998), incorporating the effects of Jupiter's oblateness up to terms in J_6. The expressions for the calculated apsidal and nodal precession rates, $\dot{\varpi}_{\rm calc}$ and $\dot{\Omega}_{\rm calc}$, respectively, were taken from Cooper and Murray (2004). The adopted reference frame is planetocentric, with x-axis corresponding to the position of

the ascending node of Jupiter's equatorial plane on the Earth mean equator of J2000. The z-axis is directed along Jupiter's spin angular momentum axis at epoch (pointing north) and the y-axis is orthogonal to x and z, and in the equatorial plane of Jupiter. The chosen epoch for the orbital solutions is 2451890.0 JED, corresponding to 2000 DEC 11 12:00:00.00 TDB. A number of key constants used in the orbit determinations are common to each solution and are described in Table 2.

Orbit fitting was performed using a least-squares differential correction technique in which the equations of condition were formed in terms of the directly observed quantities, line and sample. The measured line and sample values were corrected for phase, before being input to the orbit determination process, using the procedure described in Section 2.3. As mentioned previously, this correction is essential in order to avoid significant systematic bias in the fitted orbital parameters. Numerical solution of the equations of condition was performed using the SVD-based method of Lawson and Hanson (1975). Solutions for Amalthea and Thebe, in terms of the classical orbital elements, given by semi-major axis $a_{\rm calc}$, eccentricity e, inclination i, longitude of ascending node Ω, longitude of pericentre ϖ, mean longitude at epoch λ_0, and mean motion n are shown in Table 4. The calculated semi-major axes, $a_{\rm calc}$, were obtained by solving the standard expression for the mean motion, n, in terms of the primary body radius and the zonal harmonics, up to J_6 (see, for example, Nicholson and Porco, 1988). We mention in passing that, although the quoted errors in Table 4 are the formal 1σ values from the fitting process, the correlation matrices suggest some degree of correlation between parameters, indicating that the quoted errors may be underestimates. This is probably due to the uneven orbital coverage (Fig. 1). The poorer coverage along the apsidal line for Thebe may also explain the significantly higher uncertainty in the fitted eccentricity for Thebe, compared to Amalthea (see Fig. 1 and Table 4).

Fit residuals for the N1355 and N1358 image series are shown graphically in Figs. 2 and 3, respectively.

For comparison with the fitted RMS values quoted in Table 4, the RMS residuals for Amalthea and Thebe relative to JPL's JUP230 ephemeris were 0.306 and 0.604 pixel (equivalent to 0.378 and 0.746 arcsec), respectively.

Table 3
JPL Cassini NAC calibration results (Owen, 2003)

Parameter	Value	Units
f	2002.703	mm
ϵ_1	8.28	$\times 10^{-6}$ mm^{-2}
ϵ_2	5.45	$\times 10^{-6}$ mm^{-1}
ϵ_3	−19.67	$\times 10^{-6}$ mm^{-1}
K_x	83.33333	samples/mm
K_{xy}	0.0	samples/mm
K_{yx}	0.0	lines/mm
K_y	83.3428	lines/mm

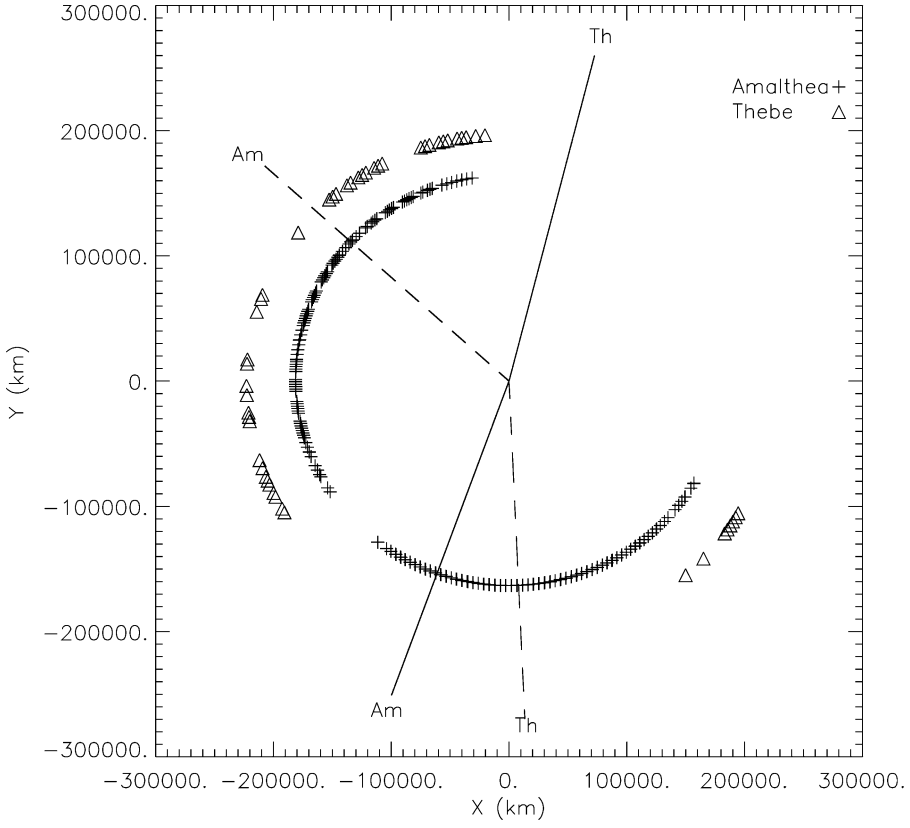

Fig. 1. Orbital coverage for the Cassini ISS NAC observations of the inner jovian satellites, Amalthea and Thebe, projected on to the equatorial plane of Jupiter, in the orbit determination reference frame (see Section 3). Solid radial lines point to fitted pericentres at epoch. Dashed radial lines point to fitted ascending nodes at epoch.

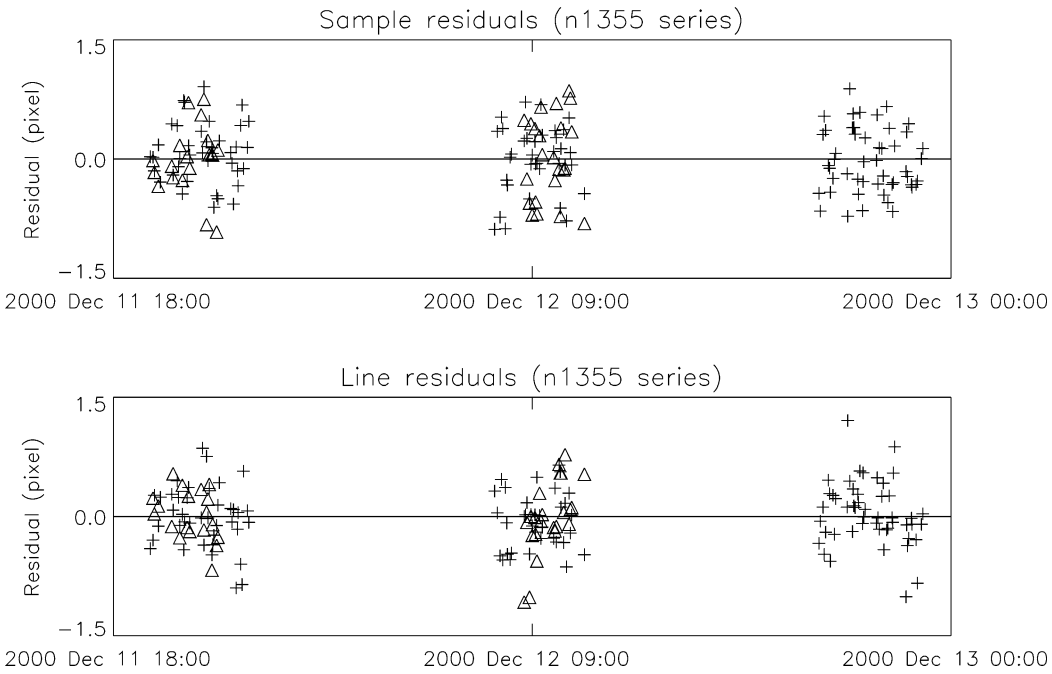

Fig. 2. Line and sample residuals for N1355 series of images. Units are NAC pixels (where 1 NAC pixel $\simeq$ 1.2357 arcsec). Amalthea values are shown by crosses and Thebe by triangles, as for Fig. 1.

Table 4
Orbital elements at 2451890.0 JED

Parameter[a]	Amalthea	Thebe
$a_{\rm calc}$ (km)	181365.84 ± 0.02	221889.0 ± 0.6
e	0.00319 ± 0.00004	0.0175 ± 0.0004
i (deg)	0.374 ± 0.002	1.076 ± 0.003
Ω (deg)	140.7 ± 0.2	273.5 ± 0.2
ϖ (deg)	248.3 ± 0.7	74.4 ± 0.3
λ_0 (deg)	241.521 ± 0.003	355.69 ± 0.02
n (deg/day)	722.6312 ± 0.0001	533.700 ± 0.002
$\dot{\varpi}_{\rm calc}$ (deg/day)	2.50987933	1.23273543
$\dot{\Omega}_{\rm calc}$ (deg/day)	−2.50119599	−1.2298952
rms[b]	0.364	0.443

[a] See Section 3 for further description of fitted parameters. All longitudes $(\Omega, \varpi, \lambda)$ measured from the ascending node of Jupiter's equator at epoch on the Earth mean equator of J2000. Inclination, (i), measured relative to Jupiter's equatorial plane. Quoted uncertainties are the formal 1σ values from the fit.

[b] Units are NAC pixels (where 1 NAC pixel $\simeq$ 1.2357 arcsec).

4. Discussion

The close dynamical and geometrical relationship between the four inner jovian satellites and the rings is now well-established (see, for example, Burns et al., 1999; Ockert-Bell et al., 1999; Porco et al., 2003). In particular, the correlation between the measured half-widths of the Amalthea and Thebe rings and the maximum vertical extents of the orbits of Amalthea and Thebe above the ring plane, lead Ockert-Bell et al. (1999) to conclude that these satellites are sources of the ring material. Repeating the calculations of Ockert-Bell et al. (1999) using the expression $z = a(1 + e)\sin i$ for the maximum vertical elevation, z, of a satellite above the equatorial plane, in terms of its semi-major axis, a, eccentricity, e and inclination, i, we obtain $z = 1188 \pm 6$ km for Amalthea and $z = 4240 \pm 12$ km for Thebe (using the fitted orbital elements from Table 4). This is consistent with the estimated half-thickness <2000 and >4000 km for the Amalthea and Thebe rings, respectively, according to Ockert-Bell et al. (1999). de Pater et al. (1999) estimate full ring thicknesses of 0.11 $R_{\rm J}$ and 0.17 $R_{\rm J}$ respectively based on Keck infrared observations, giving numerical half-widths of 3927 km and 6069 km, using the value of $R_{\rm J}$, the mean equatorial radius of Jupiter given in Table 2.

While a more detailed examination of the dynamics of Amalthea and Thebe and their relationship with the rings is beyond the scope of this paper, we hope the observations presented here will prove useful as part of any broader study, which could incorporate all existing historical astrometric observations, in addition to those presented in this work.

Acknowledgments

The authors gratefully acknowledge the many helpful comments of Bob Jacobson and Bill Owen at JPL, with special thanks to Bill Owen for details of his geometric calibration model, as described in Appendix A. Thanks also to the Cassini ISS team. In addition, Cooper and Murray express their gratitude to the UK Particle Physics and Astronomy Research Council for financial support.

Appendix A. Processing Cassini ISS astrometric observations

Here we describe the steps necessary to transform a modelled target satellite position in the Cartesian planetocentric reference frame into equivalent line and sample coordinates in a Cassini image.

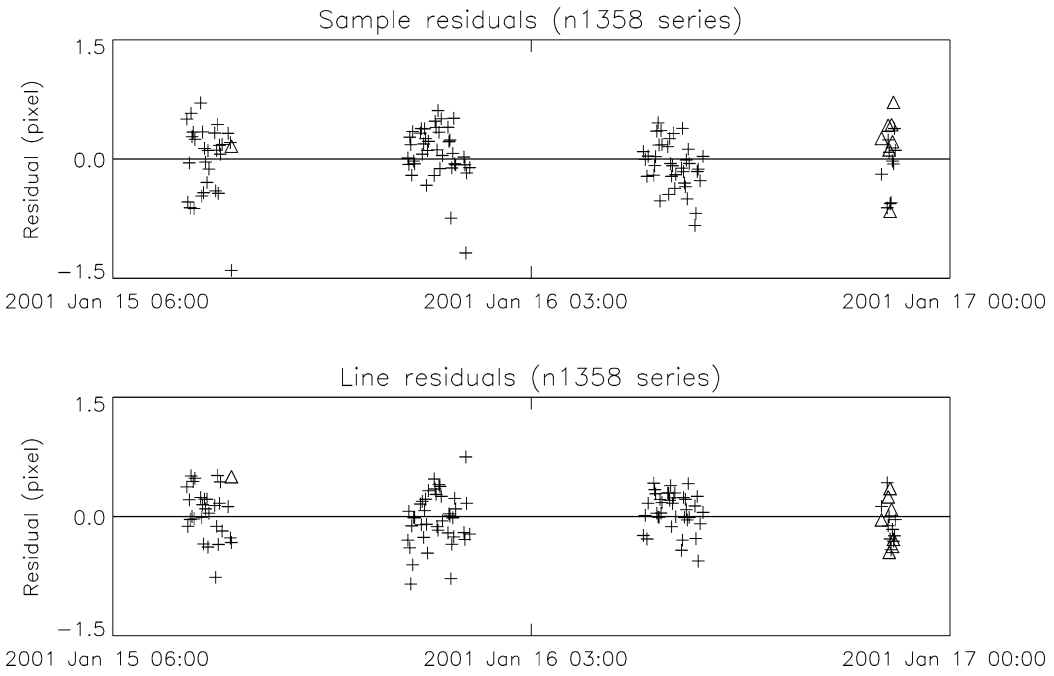

Fig. 3. Line and sample residuals for N1358 series of images. Units are NAC pixels (where 1 NAC pixel $\simeq$ 1.2357 arcsec). Amalthea values are shown by crosses and Thebe by triangles, as for Fig. 1.

1. Given α and δ, the right ascension and declination, respectively, of the pole of the primary body in the J2000 frame (Table 2), rotate the position vector of the target satellite from the planetocentric to the J2000 frame:

$$\mathbf{S}_{t-\tau} = \begin{pmatrix} S_x \\ S_y \\ S_z \end{pmatrix} = \begin{pmatrix} -\sin\alpha & \cos\alpha & 0 \\ -\cos\alpha\sin\delta & -\sin\alpha\sin\delta & \cos\delta \\ \cos\alpha\cos\delta & \sin\alpha\cos\delta & \sin\delta \end{pmatrix} \begin{pmatrix} s_x \\ s_y \\ s_z \end{pmatrix}. \quad \text{(A.1)}$$

2. Compute the pointing vector $\mathbf{p}_t$ from the Cassini spacecraft to the target satellite in the J2000 frame:

$$\mathbf{p}_t = \mathbf{S}_{t-\tau} - \mathbf{A}_{t-\tau}. \quad \text{(A.2)}$$

$\mathbf{A}_{t-\tau}$ and $\mathbf{S}_{t-\tau}$ are the position vectors of the spacecraft and target satellite, respectively, in the J2000 frame, at the one-way light-time-corrected observation time (note that this expression includes light-time and stellar aberration corrections: see, for example, Seidelmann (1992, p. 133)). The position vector for the spacecraft may be obtained from the tour kernel (Table 2) using the SPICE *spkpos* routine.

3. Rotate the unit pointing vector from the J2000 frame to the camera-body frame using the C-matrix:

$$\hat{\mathbf{P}}_t = \begin{pmatrix} P_x \\ P_y \\ P_z \end{pmatrix} = \mathbf{C}\hat{\mathbf{p}}_t, \quad \text{(A.3)}$$

where

$$\mathbf{C} = \mathbf{R}_3(\phi)\mathbf{R}_1(90^\circ - \delta)\mathbf{R}_3(90^\circ + \alpha) \quad \text{(A.4)}$$

and α, δ, and ϕ are, respectively, the nominal right ascension, declination and twist angles for the camera optical axis, in degrees (see Table 1), and $\mathbf{R}_i$ is the 3×3 rotation matrix about the ith axis.

4. Transform from the camera body frame into image coordinates (s, l), where s is sample and l is line, via the projection (following Owen, 2003):

$$\begin{pmatrix} s \\ l \end{pmatrix} = \sigma \begin{pmatrix} K_x & K_{xy} \\ K_{yx} & K_y \end{pmatrix} \begin{pmatrix} x + \Delta x \\ y + \Delta y \end{pmatrix} + \begin{pmatrix} s_0 \\ l_0 \end{pmatrix}, \quad \text{(A.5)}$$

where

$$\begin{pmatrix} x \\ y \end{pmatrix} = \frac{f}{P_z} \begin{pmatrix} P_x \\ P_y \end{pmatrix}, \quad \text{(A.6)}$$

$$\begin{pmatrix} \Delta x \\ \Delta y \end{pmatrix} = \begin{pmatrix} xr^2 & xy & x^2 \\ yr^2 & y^2 & xy \end{pmatrix} \begin{pmatrix} \epsilon_1 \\ \epsilon_2 \\ \epsilon_3 \end{pmatrix} \quad \text{(A.7)}$$

and

$$r^2 = x^2 + y^2. \quad \text{(A.8)}$$

The values of the various coefficients, including the focal length, f, were empirically derived by JPL from calibration tests, using measured catalogue star positions in specially produced images of the M35 open star cluster in Gemini (Owen, 2003). We quote their values in Table 3. It should be noted that these analyses may be repeated by JPL at intervals during the Cassini tour, in order to evaluate any possible temporal variability in the model parameters. The values given in Table 3 refer to their April 2003 analysis.

The nominal image coordinates of the optic axis, (s_0, l_0) in Eq. (A.5), must be adjusted for summed images. The optic axis coordinates for the three possible image sizes are given in Table 5, with the corresponding sizes for each image given in column 3 of Table 1. Additionally, the scale factor, σ, in

Table 5
Image coordinates of optical axis

Image size (pixels)	Optical axis (s_0, l_0)[a]
1024-by-1024	(511.5, 511.5)
512-by-512	(255.5, 255.5)
256-by-256	(127.5, 127.5)

[a] In each case, the point with coordinates (0.0, 0.0) represents the centre of the first pixel.

Eq. (A.5), must be set to either 1.0, 0.5, or 0.25, for 1024-by-1024, 512-by-512 or 256-by-256 pixel images, respectively. See Porco et al. (2004) for further information regarding the Cassini ISS system.

References

Acton, C.H., 1996. Ancillary data services of NASA's navigation and ancillary information facility. Planet. Space Sci. 44, 65–70.

Burns, J.A., Showalter, M.R., Hamilton, D.P., Nicholson, P.D., de Pater, I., Ockert-Bell, M.E., Thomas, P.C., 1999. The formation of Jupiter's faint rings. Science 284, 1146–1150.

Campbell, J.K., Synnott, S.P., 1985. Gravity field of the jovian system from Pioneer and Voyager tracking data. Astron. J. 90, 364–372.

Cooper, N.J., Murray, C.D., 2004. Dynamical influences on the orbits of Prometheus and Pandora. Astron. J. 127, 1204–1217.

de Pater, I., Showalter, M.R., Burns, J.A., Nicholson, P.D., Liu, M.C. , Hamilton, D.P., Graham, J.R., 1999. Keck infrared observations of Jupiter's ring system near Earth's 1997 ring plane crossing. Icarus 138, 214–223.

Evans, M.W., Porco, C.C., Hamilton, D., Murray, C.D., 2005. The orbits of the inner jovian satellites Metis and Adrastea. Astron. J. Submitted for publication.

Lawson, C.L., Hanson, R.J., 1975. Solving Least Squares Problems. SIAM, Philadelphia.

Nicholson, P.D., Porco, C.C., 1988. A new constraint on Saturn's zonal gravity harmonics from Voyager observations of an eccentric ringlet. J. Geophys. Res. 93 (B9), 10209–10224.

Ockert-Bell, M.E., Burns, J.A., Dauber, I.J., Thomas, P.C., Veverka, J., Belton, M.J.S., Klaasen, K.P., 1999. The structure of Jupiter's ring system as revealed by the Galileo imaging experiment. Icarus 138, 188–213.

Owen Jr., W.M., 2003. Cassini ISS Geometric Calibration of April 2003. JPL IOM 312.E-2003.

Porco, C.C., and 24 colleagues, 2003. Cassini imaging of Jupiter's atmosphere, satellites and rings. Science 299, 1541–1547.

Porco, C.C., and 19 colleagues, 2004. Cassini Imaging Science: Instrument characteristics and anticipated scientific investigations at Saturn. Space Sci. Rev. 115, 363–497.

Seidelmann, P.K. (Ed.), 1992. The Explanatory Supplement to the Astronomical Almanac. University Science Books, Sausalito.

Taylor, D.B., 1998. Determination of starting conditions for ephemerides of the uranian satellites I–V. Nautical Almanac Office Tech. Note No. 72.

Thomas, P.C., Burns, J.A., Rossier, L., Simonelli, D., Veverka, J., Chapman, C.R., Klaasen, K., Johnson, T.V., Belton, M.J.S., 1998. The small inner satellites of Jupiter. Icarus 135, 360–371.

Throop, H.B., Porco, C.C., West, R.A., Burns, J.A., Showalter, M.R., Nicholson, P.D., 2004. The jovian rings: New results from Cassini, Galileo, Voyager and Earth-based observations. Icarus 172, 59–77.